1521-009X/50/1/8–16$35.00
DRUG METABOLISM AND DISPOSITION

https://doi.org/10.1124/dmd.121.000503
Drug Metab Dispos 50:8–16, January 2022

Simulating the Selection of Resistant Cells with Bystander Killing and Antibody Coadministration in Heterogeneous Human Epidermal Growth Factor Receptor 2–Positive Tumors[S]

Bruna Menezes, Jennifer J. Linderman, and Greg M. Thurber

Departments of Chemical Engineering (B.M., J.J.L., G.M.T.) and Biomedical Engineering (J.J.L., G.M.T.), University of Michigan, Ann Arbor, Michigan

Received April 13, 2021; accepted October 4, 2021

ABSTRACT

Intratumoral heterogeneity is a leading cause of treatment failure resulting in tumor recurrence. For the antibody-drug conjugate (ADC) ado-trastuzumab emtansine (T-DM1), two major types of resistance include changes in human epidermal growth factor receptor 2 (HER2) expression and reduced payload sensitivity, which is often exacerbated by heterogenous HER2 expression and ADC distribution during treatment. ADCs with bystander payloads, such as trastuzumab-monomethyl auristatin E (T-MMAE), can reach and kill adjacent cells with lower receptor expression that cannot be targeted directly with the ADC. Additionally, coadministration of T-DM1 with its unconjugated antibody, trastuzumab, can improve distribution and minimize heterogeneous delivery. However, the effectiveness of trastuzumab coadministration and ADC bystander killing in heterogenous tumors in reducing the selection of resistant cells is not well understood. Here, we use an agent-based model to predict outcomes with these different regimens. The simulations demonstrate that both T-DM1 and T-MMAE benefit from trastuzumab coadministration for tumors with high average receptor expression (up to 70% and 40% decrease in average tumor volume, respectively), with greater benefit for nonbystander payloads. However, the benefit decreases as receptor expression is reduced, reversing at low concentrations (up to 360% and 430% increase in average tumor volume for T-DM1 and T-MMAE, respectively) for this mechanism that impacts both ADC distribution and efficacy. For tumors with intrinsic payload resistance, coadministration uniformly exhibits better efficacy than ADC monotherapy (50%–70% and 19%–36% decrease in average tumor volume for T-DM1 and T-MMAE, respectively). Finally, we demonstrate that several regimens select for resistant cells at clinical tolerable doses, which highlights the need to pursue other mechanisms of action for durable treatment responses.

SIGNIFICANCE STATEMENT

Experimental evidence demonstrates heterogeneity in the distribution of both the antibody-drug conjugate and the target receptor in the tumor microenvironment, which can promote the selection of resistant cells and lead to recurrence. This study quantifies the impact of increasing the antibody dose and utilizing bystander payloads in heterogeneous tumors. Alternative cell-killing mechanisms are needed to avoid enriching resistant cell populations.

Introduction

One of the main causes of treatment failures for therapies that target human epidermal growth factor receptor 2 (HER2) receptors is intratumoral heterogeneity, which typically leads to cancer relapse with a worse prognosis (Rye et al., 2018). The combination of incomplete cell killing and tumor heterogeneity is a widespread problem in chemotherapy that can result in selection of resistant cell populations. Residual tumor cells left from previous treatment are the major cause of tumor recurrence (Allgayer and Aguirre-Ghiso, 2008; Li et al., 2015). Finding approaches to eliminate all tumor cells is a challenging task in the development of effective treatments that avoid tumor relapse.

Antibody-drug conjugates (ADCs), such as ado-trastuzumab emtansine (T-DM1), commercially known as Kadcyla, are a type of targeted therapy approved by the US Food and Drug Administration for HER2-overexpressing breast cancer relapsed from treatment with trastuzumab (Herceptin) (Manthri et al., 2019). T-DM1 efficacy has been linked closely to HER2 expression, and its efficacy decreases with a decrease in HER2 expression (Garcia-Alonso et al., 2020). Recently, Bon et al. (2020) have shown that patients previously treated with pertuzumab (also a HER2 monoclonal antibody–targeting agent) have reduced HER2 receptor availability, which makes T-DM1 less effective as a second-line treatment for patients previously treated with trastuzumab/pertuzumab as a first-line regimen. Unfortunately, T-DM1 resistance is not limited to HER2 expression, and other forms of resistance, such as limited tissue penetration (i.e., a "binding site barrier"), defective internalization, drug efflux pumps, and reduced lysosomal proteolysis, make both acquired and intrinsic resistance a major problem (Barok et al., 2014; Hamblett et al., 2015; Rios-Luci et al., 2017; Staudacher and

This work was supported by National Institutes of Health National Institute of General Medical Sciences [Grant R35-GM128819] (to G.M.T.); National Institutes of Health National Cancer Institute [Grant R01-CA196018] Multiple Principal Investigator Award (to J.J.L.); and Department of Defense [Grant BC200857] (to G.M.T. and J.J.L.).

No author has an actual or perceived conflict of interest with the contents of this article.

dx.doi.org/10.1124/dmd.121.000503.

[S] This article has supplemental material available at dmd.aspetjournals.org.

ABBREVIATIONS: ABM, agent-based model; ADC, antibody-drug conjugate; DAR, drug-antibody ratio; DM1, emtansine; HER2, human epidermal growth factor receptor 2; K_m, Michaelis-Menten constant; MMAE, monomethyl auristatin E; P_{max}, maximum probability of cell killing; SMCC, succinimidyl 4-(*N*-maleimidomethyl)cyclohexane-1-carboxylate; T-DM1, ado-trastuzumab DM1; T-MMAE, trastuzumab-MMAE.

Brown, 2017; Garcia-Alonso et al., 2020; Hunter et al., 2020). In this study, we focus on two mechanisms of resistance: 1) reduced HER2 expression as a mechanism that impacts both tissue distribution and cellular potency and 2) payload sensitivity, which impacts cell potency without changing tumor ADC distribution.

New ADC mechanisms and administration regimens have been shown to potentially overcome some of the barriers and resistance mechanisms to treatment. Some ADCs, for example, contain linkers and payloads that are more lipophilic than the emtansine (DM1)-lysine conjugate released by T-DM1, such as DM1 (with a cleavable linker) and monomethyl auristatin E (MMAE) (Kovtun et al., 2006; Erickson et al., 2010). These payloads have the ability to enter adjacent cells by crossing the cell membranes once they are released inside ADC-targeted cells. This mechanism of uptake is known as the bystander effect. If the payload reaches a sufficient concentration, adjacent cells that cannot be directly targeted by the ADC may be killed. This has been one strategy to kill cells that are resistant due to lower receptor expression.

In addition to targeting expression heterogeneity, antibodies distribute heterogeneously because of their fast binding rates relative to diffusion (Graff and Wittrup, 2003). This effect, first observed early after the advent of monoclonal antibodies (Oldham et al., 1984) and described as a "binding site barrier" by Fujimori et al. (1989), has been seen in multiple solid tumors in the clinic (Eary et al., 1989; Scott et al., 2005; Lu et al., 2020a,b). An approach to improve heterogenous drug distribution during T-DM1 administration is coadministration with its unconjugated antibody trastuzumab. ADC monotherapy with T-DM1 at a clinical dose (3.6 mg/kg) shows that the drug is localized around blood vessels in solid tumors, and most of the tumor does not receive the treatment (Rhoden and Wittrup, 2012). As shown both in mice and in simulations, coadministration of trastuzumab and T-DM1 can improve penetration and efficacy of these therapeutics in solid tumors (Cilliers et al., 2018; Menezes et al., 2020). At the same time, this coadministration reduces the number of payloads in targeted cells [which is important for cell killing (Li et al., 2016)], thereby making these cells theoretically more susceptible to continued growth and division. However, it is not known how antibody coadministration and ADCs with bystander effects might influence the selection of more resistant cells, which can potentially alter the risk of tumor relapse.

Here, we use a validated agent-based model described previously (Menezes et al., 2020) to quantify how ADCs with bystander payloads modulate efficacy in heterogeneous solid tumors with and without coadministered antibody, specifically focusing on overall efficacy and selection of resistant cells. In particular, we ask three questions: 1) How do carrier doses and bystander effects [MMAE vs. lysine-N(epsilon)-N-succinimidyl 4-(*N*-maleimidomethyl)cyclohexane-1-carboxylate (Lys-SMCC)–DM1] impact the distribution, uptake, and efficacy of ADC treatment in tumors with heterogeneous HER2 expression? 2) Do carrier doses and bystander effects show the same influence on efficacy in heterogeneous tumors when cell sensitivity to the payload does not impact tumor distribution? And 3) how do different coadministration regimens affect the selection of resistant cells, which could lead to resistant tumor relapse?

Materials and Methods

We extended our hybrid agent-based model (ABM) framework introduced previously (Menezes et al., 2020) to incorporate additional physical and biological phenomena. Briefly, the model is comprised of cells and blood vessels that behave based on probabilistic rules and their microenvironment. The previous model described plasma dynamics (clearance and payload deconjugation), drug dynamics (intracellular processing for nonbystander payloads), and cell dynamics (e.g., cell division and cell death) that impact the tumor volume in our simulations. Cells change their state from alive to dead based on the concentration of payload bound to microtubules inside of the cell. A description of our model for the plasma dynamics, drug dynamics, and agent dynamics (cancer cell and blood vessel dynamics) can be found in the Supplemental eqs. (1–15) and accompanying text.

Here, the model is extended to include: 1) angiogenesis, allowing us to look at treatment over longer periods of time; 2) heterogeneous receptor expression and sensitivity of cancer cells to payloads; and 3) bystander payloads capable of diffusing to nearby cells. These additional features allow us to compare coadministration of T-DM1 and trastuzumab-MMAE (T-MMAE) with trastuzumab in different tumor environments (Fig. 1).

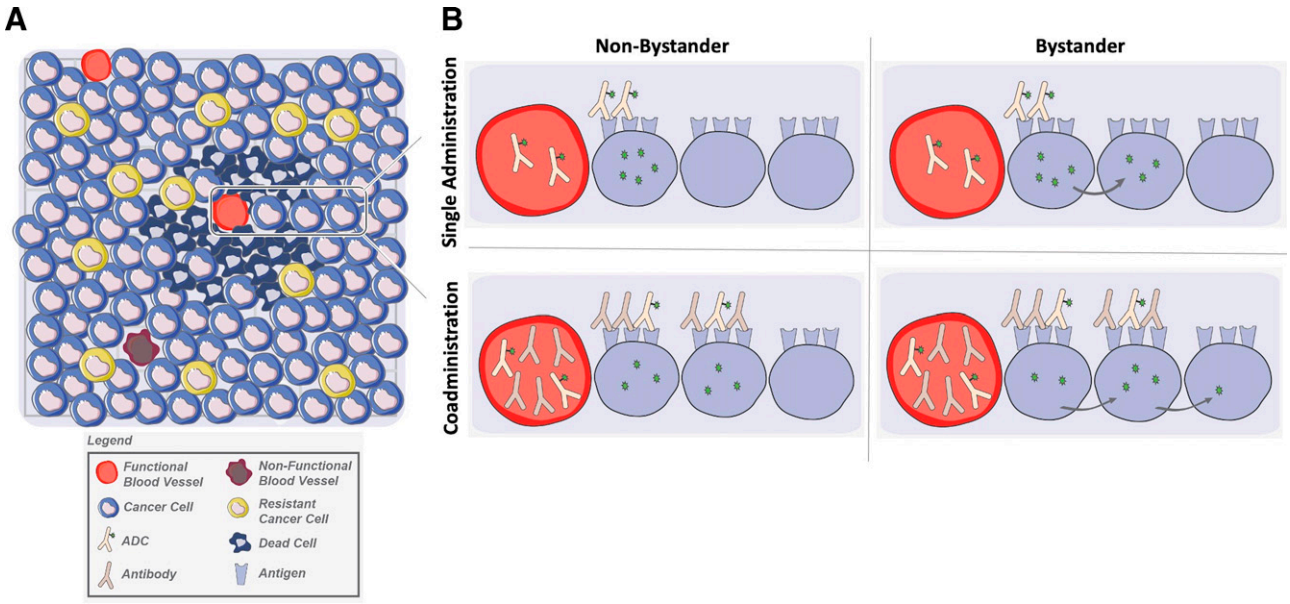

Fig. 1. Model Schematic. (A) The ABM environment is composed of cancer cells with different characteristics (e.g., different number of receptors or sensitivity to treatment) and blood vessels through which therapeutics are delivered. (B) The model tests different regimens: 1) single-agent administration (top) vs. coadministration of antibody with ADC (bottom) and 2) nonbystander payloads (left) vs. bystander payloads (right). The model can be used to examine these regimens for cell populations containing resistant cells.

Simulation Environment and Framework. The model was constructed in C++ with Boost (Boost Software License, www.boost.org). The graphical user interface was built using the Qt framework (General Public License, qt.io). Efficient linking and solution of our hybrid multiscale ABM followed the principles described in Cilfone et al. (2015) with more details in Menezes et al. (2020).

The model is a two-dimensional representation of a tumor section that contains blood vessels and several thousand cells. The cells and blood vessels have different states (i.e., alive or dead for cells and functional or nonfunctional for vessels), and they occupy specific positions on the simulation grid. Each cell occupies a volume of 2×10^{-12} l (12.6 μm on a side), and the initial tumor, which has about 1940 cells, is assumed to represent an initial tumor volume range of 200–300 mm^3. ADCs enter the tumor through active blood vessels, and the functional vessel density changes based on the tumor size. Cells were assigned either 1 million (similar to sensitive cell lines like human-derived gastric carcinoma NCI-N87) or 50,000 receptors/cell (similar to resistant cell lines like human-derived breast carcinoma JIMT-1) (Le Joncour et al., 2019), and the fraction of cells in each category could be varied. Placement of cells with either receptor number was random on the grid.

ADC Dynamics with Bystander Effects. For distribution studies, drugs are administered as a single administration on day 0, and their dynamics inside the host are described with ordinary and partial differential equations. We previously described drug dynamics with bystander effects within a Krogh cylinder model, which assumes all cells have identical properties (Khera et al., 2018), and we used these same equations (with a more sophisticated geometry) in our ABM model here. Briefly, as shown in Supplemental Fig. 1, T-DM1, T-MMAE, and trastuzumab are cleared from the plasma biexponentially, while they can at the same time extravasate into the tumor, diffuse through the interstitial tissue, bind to HER2 receptors, and internalize. After ADCs are degraded in lysosomes, the payloads Lys-SMCC-DM1 from T-DM1 and MMAE from T-MMAE enter the cytoplasm and either bind to microtubules or leave the cell. Both payloads in the interstitial tumor tissue also have the ability to enter cancer cells directly but at different rates determined by their individual properties.

Vessel Dynamics. Although tumors form new blood vessels to sustain tumor growth (angiogenesis), the functional or active vessel density is also known to decrease with increasing tumor size (Hilmas and Gillette, 1974; Williams et al., 1988). In our model, grid locations for blood vessels (functional and nonfunctional) were identified before the start of simulations. The initial densities of total and active blood vessels were calibrated as described in Menezes et al. (2020). At each agent time step, new blood vessels can become functional as tumor size increases, but the overall vessel density (vessels per tumor volume) decreases (i.e., the tumor volume grows faster than vessel density). This is done by calculating the fraction of active blood vessels at each agent time step and comparing it with the tumor volume at that time and with its initial fraction of active blood vessels set at the beginning of the simulation as shown in eq. 1:

$$fr_t = fr_o \left(\frac{V}{V_0}\right)^{-a} \tag{1}$$

where fr_t is the active fraction of blood vessels at the agent time step, fr_o is the active fraction of blood vessels assigned at the beginning of the simulation, V is tumor volume at the agent time step (mm^3), and V_0 is the initial tumor volume (mm^3). The parameter a was fit to experimental data and has a value of 0.28 (Supplemental Fig. 2) (Hilmas and Gillette, 1974). With this method, the overall decrease in active vessel density that occurs at the same time that new blood vessels are formed during the increase in tumor volume is captured.

Cell Dynamics and Model Calibration. Cells proliferate and die as the simulation progresses. All cells in the tumor in a particular simulation proliferate with the same doubling time, with doubling times chosen from 5–17 days based on calibration to experimental data (Cilliers et al., 2018). Cancer cells change their states from alive to dead based on the concentration of payloads bound to microtubules inside the cell. The probability of cell killing per agent time step is:

$$P_{kill} = \frac{P_{max}\ [P_b]}{K_m + [P_b]} \tag{2}$$

where P_{max} is the maximum probability of cell killing, $[P_b]$ is the concentration of payload bound to microtubules in nanomolar, and K_m is the Michaelis-Menten constant in nanomolar.

In Vivo Efficacy in a Xenograft Model. All animal studies were conducted according to University of Michigan Institutional Animal Care and Use Committee. For fractionated dosing, NCI-N87 cells were purchased from American Type Culture Collection (Manassas, VA) and grown at 37°C with 5% CO in RPMI 1640 growth medium supplemented with 10% (v/v) FBS, 50 U/ml penicillin, and 50 μg/ml streptomycin. Mycoplasma testing was performed annually using the MycoAlert Testing Kit (NC971983; Thermo Fisher Scientific, Waltham, MA). For the xenograft studies, 5×10^6 NCI-N87 cells were inoculated in the rear flank of 4–8-week-old female nude (Foxn1 nu/nu) mice from The Jackson Laboratory. Tumors were measured with calipers every other day, and the tumor volume was calculated as length × $width^2/2$. When tumors reached approximately 250 mm^3, three doses of T-DM1 at 2.4 mg/kg were given at days 0, 7, and 14. Tumors were monitored until the tumor reached 2000 mm^3 or ulcerated.

Results

Model Calibration and Validation. This model used pharmacokinetic parameters estimated based on physicochemical properties and a previous publication by Khera et al. (2018) (see Supplemental Tables 1 and 2). Cell doubling time was calibrated to published data (Cilliers et al., 2018) as previously shown in Menezes et al. (2020), giving a range of 5–17 days. The cell-killing parameters P_{max} and K_m were herein calibrated and validated for Lys-SMCC-DM1 (T-DM1) and MMAE (T-MMAE) using experimental data from Cilliers et al. (2018) and Singh et al. (2020a,b) along with CaliPro, our calibration protocol for parameter estimation (Joslyn et al., 2020). For Lys-SMCC-DM1, cell-killing calibration is shown in Supplemental Fig. 3A with P_{max} and K_m 0.0014 and 800, respectively, and validated in Supplemental Fig. 3, B–D. For MMAE, P_{max} and K_m were 0.006 and 600, respectively, for calibration as shown in Supplemental Fig. 4A and validated in Supplemental Fig. 4, B–D.

Once the model was calibrated and validated to the pharmacodynamic data, the results were compared with in vivo efficacy data collected after fractionated dosing with three doses of 2.4 mg/kg of T-DM1 (3 × 2.4 mg/kg) as illustrated in Supplemental Fig. 5. As shown in Supplemental Fig. 5B, the addition of angiogenesis better fits the experimental data with fractionated doses compared with our previous version of the model (Supplemental Fig. 5A) with static vessel distribution.

Bystander Payload Reaches More Cells Albeit at Lower Concentrations per Cell. To compare delivery of bystander and nonbystander payloads to tumor cells, the payload concentrations of MMAE and Lys-SMCC-DM1 were quantified by simulating the distribution and uptake of ADCs and their respective payloads for 3.6 mg/kg of T-DM1 with drug-to-antibody ratio (DAR) 3.5 (clinical dose) and 1.8 mg/kg of T-MMAE with DAR 4. The results shown in Fig. 2 reflect the maximum peak that occurs at day 1 (24 hours) for ADCs bound to the cell surface and at day 4 for microtubule-bound payload. T-DM1 at 3.6 mg/kg reaches more cells at day 1 than T-MMAE at 1.8 mg/kg does, which is consistent with increased penetration of a higher antibody dose. However, the MMAE payload reaches more cells at day 4 than Lys-SMCC-DM1 does (Fig. 2, C and D), which is consistent with previous results from our Krogh cylinder model and as expected given the bystander effects for MMAE (Ilovich et al., 2018; Khera et al., 2018).

The single-cell analysis capabilities of our ABM were used to quantify the penetration of MMAE in comparison with Lys-SMCC-DM1 as measured by the percentage of cells with high (≥150 nM), moderate (150 nM > x ≥ 1 nM), and low payload concentrations (<1 nM) (Li et al., 2016) (Fig. 2E). We also examined two additional scenarios (3 mg/kg and DAR 3 for both T-DM1 and T-MMAE to match the dose and DAR for a more direct comparison of the ADCs), as shown in Supplemental Fig. 6. For T-MMAE administration, all cells are reached by MMAE, and the majority of cells receive concentrations between 150 and 1 nM. In contrast, Lys-SMCC-DM1 reaches fewer cells, and

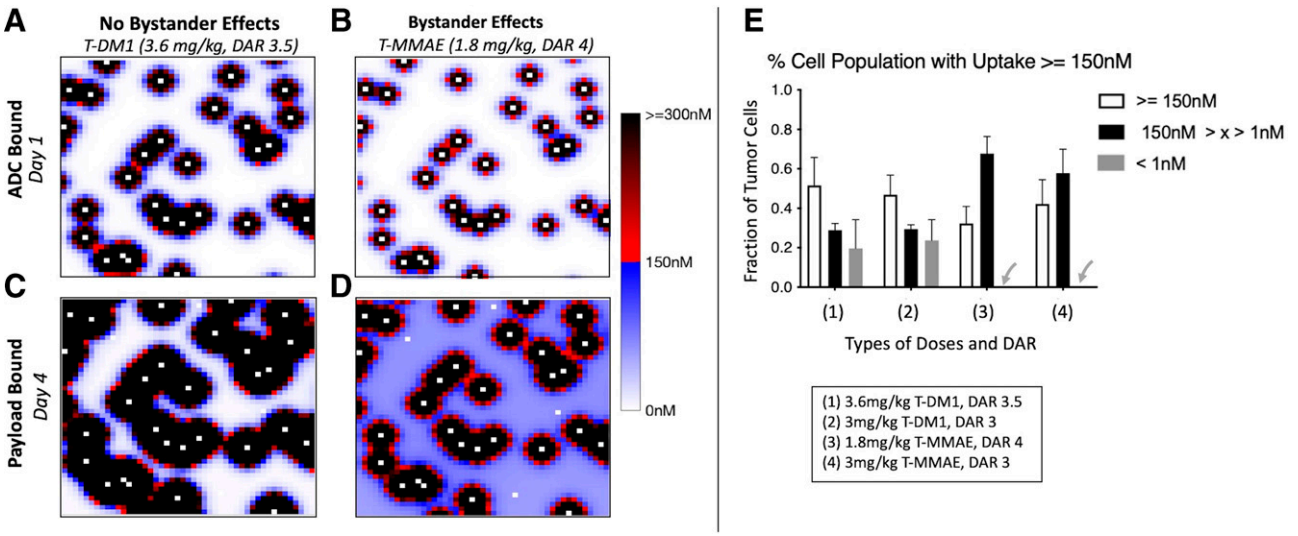

Fig. 2. Similar ADC penetration but greater payload distribution of T-MMAE. (A and B) Distribution of T-DM1 (3.6 mg/kg with DAR 3.5) and T-MMAE (1.8 mg/kg, DAR 4) bound on the surface of the cancer cells. (C and D) Distribution of Lys-SMCC-DM1 and MMAE bound to microtubules inside the cells. (E) Percentage of cells with high- (≥150 nM), moderate- (150 nM > x ≥ 1 nM), and low-payload concentrations (<1 nM) at day 4, the time of maximum payload uptake. n = 10 simulations, with mean and S.E.M. shown. T-MMAE has no cells with payload concentration <1 nM (shown by the gray arrows). Supplemental Fig. 6 shows the comparison between these two ADCs for the same dose and DAR; both ADCs reach the same number of cells at day 1, but the MMAE payload again reaches more cells at day 4.

the majority of targeted cells receive concentrations higher than 150 nM. Many cells in T-DM1 administration receive very little Lys-SMCC-DM1, demonstrating a more heterogeneous distribution (Fig. 2E). These data capture the bystander effect of payloads, such as MMAE, that reach more cells but have lower concentrations than a nonbystander payload, which is a consequence of the payload's lipophilicity and ability to diffuse into adjacent cells.

Antibody Coadministration Reduces Efficacy in Tumors with Low Receptor Expression. To compare how coadministration of trastuzumab with T-DM1 or T-MMAE impacts the efficacy in tumors with cell populations with heterogeneous receptor expression (vs. a base case of uniform high expression), we simulated tumors with varying fractions of cells with 1 million or 50,000 receptors/cell and treated them with trastuzumab to ADC dose ratios of 0:1, 3:1, and 8:1, dosing every 21 days (days 0, 21, and 42). The average tumor volumes at 50 days for administration of T-DM1 at 3.6 mg/kg (DAR 3.5) and T-MMAE at 1.8 mg/kg (DAR 4) are shown in Fig. 3. In tumors with 60%–100% of cells expressing 1 million receptors, adding a carrier dose improves the efficacy for T-DM1 and T-MMAE (up to 70% and 40% decrease in average tumor volume, respectively). In tumors with a majority of cells having lower receptor numbers (0%–20% with 1 million receptors), coadministration reduces efficacy (up to 360% and 430% increase in average tumor volume for T-DM1 and for T-MMAE, respectively), and administration of ADC alone is more efficacious. The poor efficacy of coadministration with heterogeneous expression is similar to that for tumors with uniformly low receptor expression. When most cells express only a low number of receptors, ADCs distribute more evenly in the tumor than they do for high receptor expression, which increases efficacy. Adding

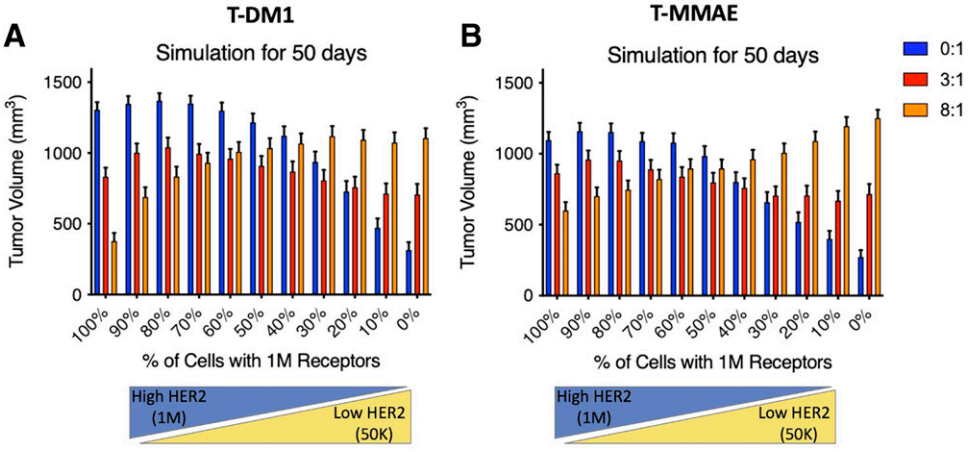

Fig. 3. Treatment efficacy at 50 days for tumors with heterogeneous receptor expression. (A) T-DM1 regimens (3.6 mg/kg and DAR 3.5) and (B) T-MMAE regimens (1.8 mg/kg and DAR 4) for tumors with changing percentage of 1 million (1M) or 50,000 (50K) receptors/cell for administration every 21 days (at days 0, 21, and 42). Data (mean and S.E.M.) are shown for n = 100 simulations. As the number of receptors decreases, coadministration of 8:1 antibody reduces efficacy. These data also show the larger benefit of coadministration for ADCs with nonbystander payloads that cannot diffuse deeper into the tissue to partially compensate for heterogeneous distribution. For tumors with uniformly high expression, the addition of 3:1 and 8:1 carrier doses to T-DM1 reduces tumor growth by a larger amount than those for T-MMAE.

unconjugated antibody to the regimen (coadministration) puts the unconjugated antibody in competition with ADCs, and cells with fewer receptors do not internalize sufficient ADC for cell killing, which lowers efficacy.

The trade-off between improved tissue distribution (pharmacokinetics) and targeted cell killing (pharmacodynamics) is highlighted in the shift of cell populations with high, moderate, and low levels of payload uptake. Supplemental Fig. 7 quantifies the percentages of cells with different payload concentrations. These simulations show an increase in the fraction of cells with high payload delivery for the 0:1 regimen, since the average receptor expression drops and tissue penetration increases, versus a decrease in payload delivery for the 8:1 regimen.

Bystander Effects Mitigate Loss in Efficacy from Coadministration at Low Receptor Expression. To better understand the role of MMAE bystander effects on T-MMAE efficacy, we simulated the distribution and efficacy of T-MMAE while artificially removing the payload's ability to enter adjacent cells. We performed simulations with varying receptor expression, similar to Fig. 3, and we set the internalization rate constant of MMAE to enter adjacent cells to zero as shown on Fig. 4. Comparing the distribution of Fig. 4E with control (Fig. 4B), the elimination of payload entering adjacent cells reduces the MMAE uptake in bystander cells as expected. The tumor growth curves show modestly improved responses when bystander effects are included, with significant improvement for high coadministered doses with low receptor expression, in which bystander effects help retain payload concentrations at an effective level.

Coadministration Improves Efficacy in Tumors with Intrinsically Resistant Cells. Not all mechanisms of drug sensitivity impact distribution. We simulated tumors with cell populations that are naturally more resistant to treatment (using a higher value of K_m; eq. 2) and predicted how coadministration affects tumor response. For these cells, K_m was doubled (K_m = 2x) or quadrupled (K_m = 4x), and simulations with varying percentages of more sensitive cell populations with and without coadministration are shown in Fig. 5. For T-DM1, 3:1 or 8:1 antibody coadministration improves efficacy compared with ADC alone; increasing the percentage of resistant cells uniformly reduces efficacy (Fig. 5, A and B). For T-MMAE, coadministration for tumors with a high fraction of sensitive cells also shows the benefit of the carrier dose. However, as the percentage of cells with intrinsic resistance increases, the benefit of the carrier dose is less evident. This is because of the high "dilution" of T-MMAE with trastuzumab, which affects the ability to kill those more resistant cells that require a higher concentration of the payload despite better tissue penetration reaching more cells.

Regimens with Greater Efficacy Can Select for More Resistant Cells. Next, we questioned whether bystander or nonbystander payloads and different coadministrations could select for a small number of less-sensitive cells that might then repopulate the tumor. Simulations were performed in which the initial tumor was composed of 1% cells with lower receptor expression (Fig. 6, A–F) or intrinsic resistance (value of K_m 2x) (Fig. 6, G–L). Simulations were conducted for 100 days with dosing every 3 weeks to provide time for the resistant cells to overtake the tumor, which resulted in larger tumor sizes. In general, as the ratio of trastuzumab to ADC increases, efficacy is increased for both T-DM1 and T-MMAE administration in heterogenous receptor–expressing tumors. However, resistant cells become a larger percentage of the tumor in several scenarios, showing the selection of resistant cells. The selection is highest for a nonbystander payload (T-DM1) at the highest coadministration dose (8:1). Notably, this is also the most effective treatment. T-MMAE improved efficacy with higher coadministration for tumors with differences in receptor expression, but it also showed

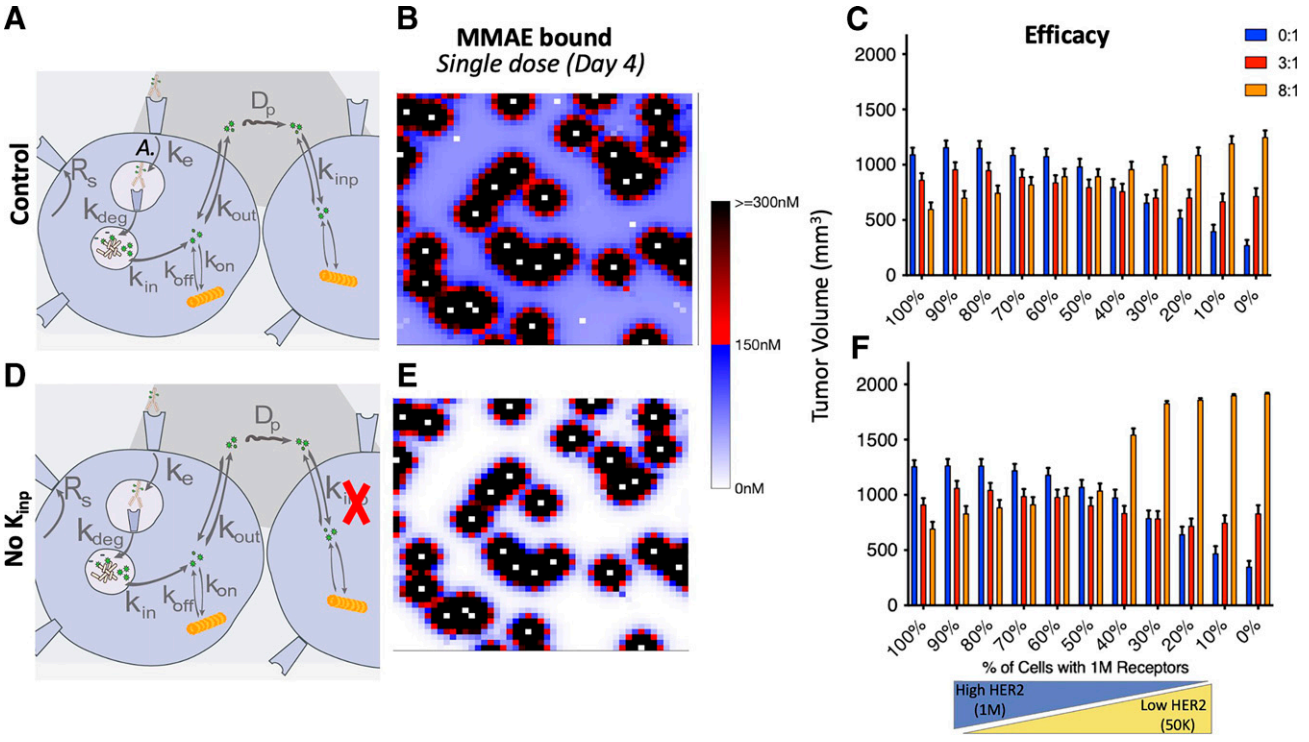

Fig. 4. Artificially removing bystander effects with coadministration changes payload distribution and efficacy. (A–C) Distribution and efficacy for regimens with T-MMAE exhibiting the expected bystander killing. (D–F) Distribution and efficacy for regimens of T-MMAE when setting the internalization rate of free MMAE (k_{inp}) to zero with different coadministration regimens. Simulations show mean and S.E.M. for n = 100 simulations. For MMAE payload, the elimination of bystander effects with high coadministrations leads to lower efficacy. Regimens tested are as in Fig. 3. 1M, 1 million; 50K, 50,000; k_{deg}, ADC degradation rate constant; k_e, endocytosis/internalization rate constant; k_{in}, payload transport rate constant into cytosol; k_{off}, payload dissociation rate constant; k_{on}, payload binding rate constant; k_{out}, payload transport rate constant out of cell; R_s, antigen synthesis rate.

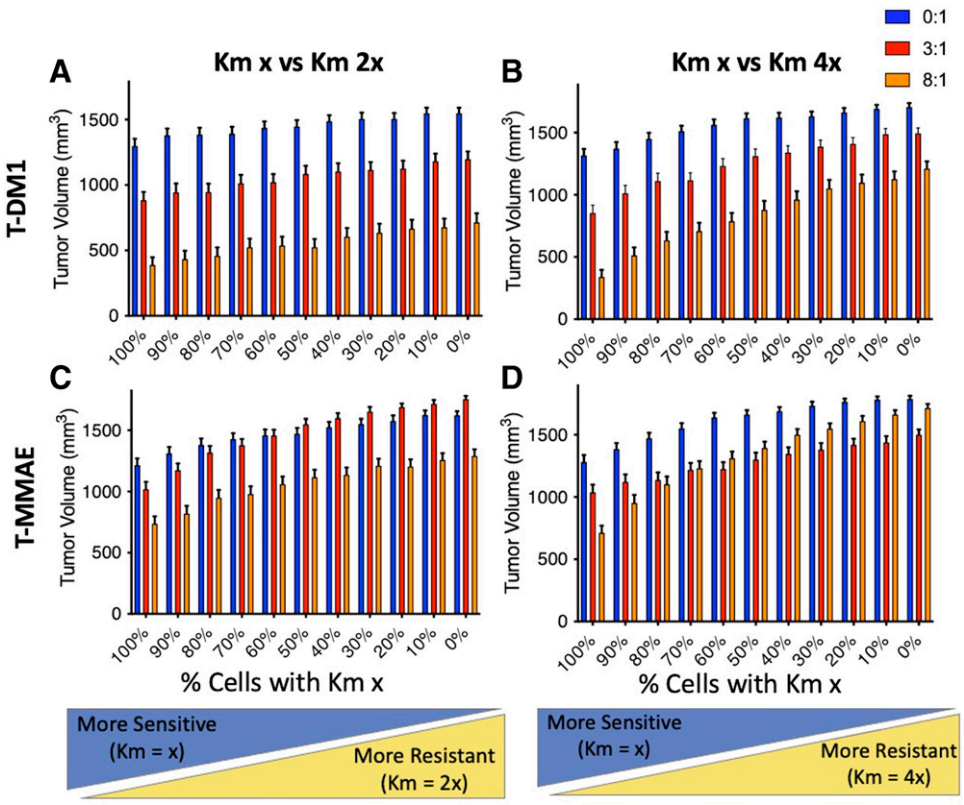

Fig. 5. Efficacy of T-DM1 and T-MMAE coadministration regimens when a fraction of cells have less sensitivity to drug. Regimens with T-DM1 (A and B) or T-MMAE (C and D) with coadministration were simulated. Tumors contained varying fractions of cells with intrinsic resistance (K_m = 2x, or K_m = 4x the value in Supplemental Table 2). Lower cell payload sensitivity impacts most regimens in a similar fashion, reducing the overall efficacy regardless of the carrier dose or bystander effects. Simulations show mean and S.E.M. for n = 100 simulations. Regimens tested are as in Fig. 3.

selection of resistant cells with coadministration. These simulations indicate that bystander killing alone may not be sufficient to prevent the outgrowth of resistant cells at clinical doses with or without a carrier dose.

MMAE exhibits bystander effects that allow the drug to diffuse more homogeneously through the tumor, but it also decreases the single-cell uptake. For intrinsic resistance that requires a higher concentration of the payload, T-MMAE here at 1.8-mg/kg dose was not effective. Since bystander effects result in lower concentrations in cells than directly targeted cells, many of the intrinsically resistant cells distant from vessels do not receive a lethal dose.

Another important observation in these data is that a large number of simulations (e.g., 100) were needed to discern trends in the results. When only 10 simulations were used, the trends seen in Fig. 6 were masked by tumor variability (unpublished data). This suggests that many samples must be taken to identify the most effective treatment, which may not be feasible with animal experiments alone. These results highlight the need for computational approaches to complement experimental results to better predict clinical outcomes.

Discussion

The clinical success of ADCs has improved in the past few years, including the increased reliance on bystander payloads and higher antibody doses. The main goal of next-generation ADCs is to improve the therapeutic index of these drugs by increasing efficacy while maintaining relative safety (Coats et al., 2019). This could be achieved by 1) increasing the delivery to more cells within the tumor, 2) utilizing bystander payloads with balanced physicochemical properties to reach nearby cells at sufficient concentrations while avoiding extensive tumor washout, and 3) driving immune responses to leverage additional mechanisms of cell killing. In this work, we concentrated on the first two approaches with a particular focus on heterogeneous tumors. Overcoming ADC delivery challenges, such as the binding site "barrier" and heterogeneous receptor expression, requires strategies, including the use of bystander payloads and higher antibody doses (e.g., coadministration regimens) to reach cells that may not be directly targeted by ADCs like T-DM1 (Yardley et al., 2015; Garcia-Alonso et al., 2020; Ocana et al., 2020). These approaches have the potential to significantly impact responses and may explain the efficacy of trastuzumab deruxtecan in gastric cancer versus T-DM1. Although both are approved for use in breast cancer, the former drug is given at higher antibody doses (6.4 vs. 3.6 mg/kg), which increases tissue penetration, and contains a bystander payload to reach low-expressing cells given the higher heterogeneity of HER2 expression in gastric cancer (Thuss-Patience et al., 2017).

Here, we used our updated hybrid agent-based model to predict the efficacy of various dosing strategies of ADCs with bystander or nonbystander payloads in heterogeneous tumors (specifically heterogeneous receptor expression and intrinsic cellular resistance). Our model presents an advantage over previous models because it includes single-cell heterogeneity, drug responses, high-resolution tuning of cancer cell and blood vessel dynamics, and heterogeneous ADC and payload delivery that are not achievable with commonly used compartmental or Krogh cylinder models.

Bystander payloads vary in lipophilicity and potency, which affects both the ADC's pharmacokinetics and pharmacodynamics. For example, MMAE has increased lipophilicity compared with that of Lys-SMCC-DM1, with a calculated partition coefficient clogD of 2.01

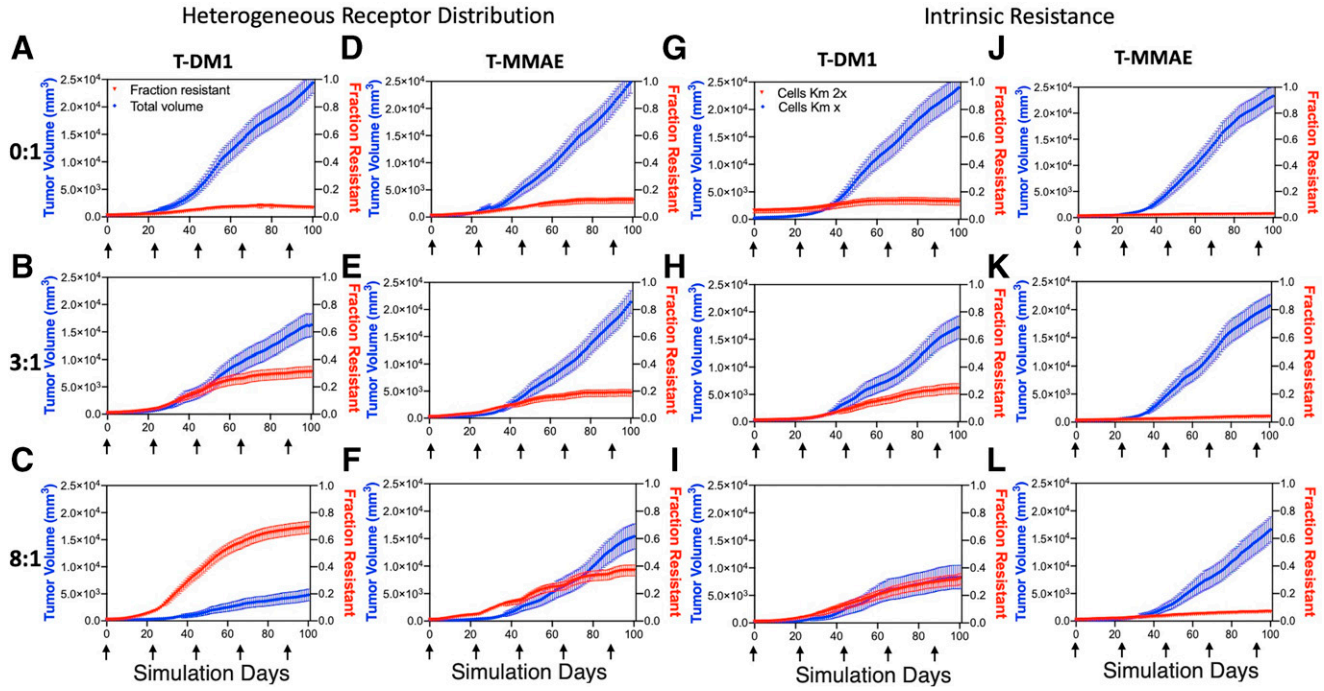

Fig. 6. Tumor growth with initial composition of 1% of resistant cells vs. sensitive cells for different regimens with T-DM1 or T-MMAE. (A–F) Coadministration of trastuzumab 0:1, 3:1, and 8:1 with T-DM1 (A–C) and T-MMAE (D–F) every 3 weeks (marked by arrows) initially containing 1% of tumor cells with 50,000 receptors/cell vs. 99% of 1 million receptors/cell. (G–L) Coadministration of trastuzumab 0:1, 3:1, and 8:1 with T-DM1 (G–I) and T-MMAE (J–L) every 3 weeks initially containing 1% of cells with higher intrinsic resistance (K_m = 2x) vs. 99% of cells with K_m = 1x. K_m = 800 nM for T-DM1, and K_m = 600 nM for T-MMAE. Simulations show mean and S.E.M. for n = 100 simulations. In most cases, more effective treatments result in a larger fraction of resistant cells.

versus 1.21, respectively (Khera et al., 2018). This changes how easily payloads cross cell membranes, how much they nonspecifically adhere to proteins and membranes inside and outside the tumor cells, and how effectively they diffuse through the tumor tissue. As seen in Fig. 2, C and D (and Supplemental Fig. 6, C and D), this helps MMAE penetrate deeper and more homogeneously into the tissue, whereas Lys-SMCC-DM1 has a more heterogeneous distribution influenced exclusively by the penetration depth of the intact ADC. MMAE, on the other hand, does not accumulate to sufficient levels for complete cell killing inside cells reached via the bystander effect at the doses given here (1.8 mg/kg), but for higher doses like 3.6 mg/kg, the payload reaches cells with concentrations shown to be effective (Singh et al., 2016, 2020a). Other payloads, such as deruxtecan, have shown significant bystander killing at clinically tolerable doses (Ogitani et al., 2016). These agents may be able to better target antigen-negative cells than the payloads used here, which is important for clinically heterogeneous tumors (Seol et al., 2012). Singh et al. (2020b) emphasized the importance of a parallel decline in antigen-positive and antigen-negative cells within a heterogeneous tumor in order to maintain bystander killing. The higher efficiency of direct cell killing relative to bystander killing may make this difficult to achieve in practice (Khera et al., 2018).

Because of MMAE's relatively high potency, reduced efficacy from the bystander escape of the payload and loss in concentration (washout) are only evident in high trastuzumab ratios and tumors with low total receptor expression (e.g., <30% 1M; Fig. 4F). Other very potent bystander payloads, such as pyrrolobenzodiazepine and indolinobenzodiazepine dimers (DNA alkylators), are also very lipophilic and have demonstrated optimal bystander efficiency by balancing the difference between retention and diffusion through cells, which can minimize washout of the drug from the tumor (Khera et al., 2018, 2021). However, these potent payloads must be administered at lower doses than microtubule inhibitors because of their toxicity.

In general, T-DM1 and T-MMAE efficacy benefit from coadministration with trastuzumab for tumors with high receptor expression, but the benefit of coadministration is reduced and eventually lost for tumors with lower receptor expression as shown in Fig. 3. Consistent with previous work, coadministration offers advantages for T-MMAE in high-expression tumors, since the efficiency of direct cell targeting is greater than bystander killing (Khera et al., 2018; Singh et al., 2020a). Figures 3 and 4 highlight the need for a balance between fast escape of the payload versus accumulation in cells to mediate cell death. Approaches that enable fast endosomal/lysosomal escape but prevent cellular escape/washout (similar to the dolaflexin payload) could increase potency by locking the toxic payload inside of the cytosol (Clardy et al., 2018). The higher efficacy of T-DM1 and T-MMAE with increasing numbers of low-expressing cells may seem counterintuitive. However, this result, in which lower receptor expression improves efficacy because of better tissue penetration, has been observed experimentally (Nessler et al., 2020; Ponte et al., 2021).

Other diverse mechanisms of resistance can lead to intrinsic cellular resistance wherein cells require a higher concentration of drug for cell killing (Barok et al., 2014). We performed simulations to understand how coadministration of antibody with ADCs carrying bystander and nonbystander payload in the presence of these resistant cells modulates efficacy. In general, the results in Fig. 5 show that coadministration is better for the vast majority of tumor compositions when the resistance mechanism does not influence tumor distribution. A few tumor compositions with a very high concentration of resistant cells (right side of Fig. 5, C and D) show similar efficacy regardless of carrier dosing, but these regimens are ineffective overall. Strategies, such as interchanging payloads (van Geel et al., 2015), may be needed to restore cellular sensitivity in these cases. The benefit of the carrier dose is greater for T-DM1 than T-MMAE because of the ability of bystander payloads to partially compensate for heterogeneous tissue penetration. When the

resistance mechanism does not influence distribution, the carrier dose is more consistently beneficial with fewer trade-offs.

In these simulations, we also saw that the regimens that led to better efficacy also led to selection of more resistant cells (Fig. 6C). These dynamics highlight fundamental limitations in improving efficacy by only taking into consideration changes in dosing regimens of ADCs. Although these approaches are beneficial for a period of time, tumor reoccurrence could result in a short duration of response (Banerjee et al., 2018) and potentially lead to an even more resistant tumor composition. This work highlights the need to use other mechanisms of action and treatments, similar to combination therapy used with current chemotherapeutics. This could include efforts to mitigate specific mechanisms of resistance, such as selecting payloads that are less susceptible to drug exporters, or more broadly effective approaches, including the stimulation of an immune response.

This model, like other preclinical models, encounters some limitations in the translation to the clinical setting. For example, many clinical tumor parameters are infeasible to measure, although progress is being made (Lu et al., 2020a,b), and the translation to the clinic requires estimation of these parameters with adjustment for species (Shah et al., 2012; Singh and Shah, 2017). Additional features beyond scaling clearance rates are needed to capture human plasma pharmacokinetics of drugs like T-DM1, such as ADC deconjugation, TMDD, and HER2 shedding (Betts et al., 2020). Finally, stromal cells (including immune cells) can play a major role in response (Rios-Doria et al., 2017; Iwata et al., 2018; D'Amico et al., 2019). Although these features are not important in this mouse model and therefore were not included here, they are important for plasma clearance and tumor response in humans.

This last result and the ability of cells to escape payload killing highlight how more effort should be spent on understanding and developing agents capable of immune stimulation, and for this reason, future work with hybrid ABMs should include immune cells and other molecules. In particular, many ADCs have demonstrated immunostimulatory effects, including benefits from combination therapy with checkpoint inhibitors and immune cell agonists. For example, antibody mechanisms of action, such as antibody-dependent cellular cytotoxicity, could also help eradicate cells with lower HER2 expression that have lost sensitivity to receptor signaling blockade (Barok et al., 2007). By including these additional dynamics in the tumor microenvironment, these simulations could help guide the overall development of ADC therapies.

Computational approaches provide a powerful tool to aid ADC development when combined with experimental work (Vasalou et al., 2015; Maass et al., 2016; Khera et al., 2018; Byun and Jung, 2019; Singh et al., 2020b). For example, in vitro experiments alone lack the tissue penetration issue that animal results and computational methods can capture for better clinical predictions (e.g., Cilliers et al., 2016, 2018). Animal experiments also have significant limitations, such as high tolerability and faster pharmacokinetics than humans, which results in overdosing many animal experiments relative to the clinical and obscuring delivery challenges in vivo. Nonhuman primate toxicity studies are needed for crossreactivity to ADCs, but these animals lack tumors, so the interplay of toxicity and efficacy cannot be determined (Ponte et al., 2021). The limitations of experiments can be addressed by calibrated and validated computational approaches that capture the in vitro and in vivo efficacy, toxicity, and scaling challenges in a single system. In addition, computational approaches provide the power to discern trends that may be lost in the noise during animal studies with small cohort sizes. These trends may not appear until later during development when larger studies and clinical trials are conducted. In contrast, a large number of simulations (e.g., $n = 100$) can more efficiently identify trends in the outcomes. This supports the use of computer simulations, especially with ABMs, as an approach to help streamline the development of ADCs.

Authorship Contributions

Participated in research design: Menezes, Linderman, Thurber.

Conducted experiments: Menezes.

Performed data analysis: Menezes, Linderman, Thurber.

Wrote or contributed to the writing of the manuscript: Menezes, Linderman, Thurber.

Acknowledgments

The authors thank Paul Wolberg for technical assistance.

References

Allgayer H and Aguirre-Ghiso JA (2008) The urokinase receptor (u-PAR)—a link between tumor cell dormancy and minimal residual disease in bone marrow? *APMIS* **116**:602–614 DOI: 10.1111/j.1600-0463.2008.00997.x.

Banerjee S, Oza AM, Birrer MJ, Hamilton EP, Hasan J, Leary A, Moore KN, Mackowiak-Matejczyk B, Pikiel J, Ray-Coquard I, et al. (2018) Anti-NaPi2b antibody-drug conjugate lifastuzumab vedotin (DNIB0600A) compared with pegylated liposomal doxorubicin in patients with platinum-resistant ovarian cancer in a randomized, open-label, phase II study. *Ann Oncol* **29**:917–923 DOI: 10.1093/annonc/mdy023.

Barok M, Isola J, Pályi-Krekk Z, Nagy P, Juhász I, Vereb G, Kauraniemi P, Kapanen A, Tanner M, Vereb G, et al. (2007) Trastuzumab causes antibody-dependent cellular cytotoxicity-mediated growth inhibition of submacroscopic JIMT-1 breast cancer xenografts despite intrinsic drug resistance. *Mol Cancer Ther* **6**:2065–2072 DOI: 10.1158/1535-7163.MCT-06-0766.

Barok M, Joensuu H, and Isola J (2014) Trastuzumab emtansine: mechanisms of action and drug resistance. *Breast Cancer Res* **16**:209 DOI: 10.1186/bcr3621.

Betts A, Clark T, Jasper P, Tolsma J, van der Graaf PH, Graziani EI, Rosfjord E, Sung M, Ma D, and Barletta F (2020) Use of translational modeling and simulation for quantitative comparison of PF-06804103, a new generation HER2 ADC, with Trastuzumab-DM1. *J Pharmacokinet Pharmacodyn* **47**:513–526 DOI: 10.1007/s10928-020-09702-3.

Bon G, Pizzuti L, Laquintana V, Loria R, Porru M, Marchiò C, Krasniqi E, Barba M, Maugeri-Saccà M, Gamucci T, et al. (2020) Loss of HER2 and decreased T-DM1 efficacy in HER2 positive advanced breast cancer treated with dual HER2 blockade: the SePHER Study. *J Exp Clin Cancer Res* **39**:279 DOI: 10.1186/s13046-020-01797-3.

Byun JH and Jung IH (2019) Modeling to capture bystander-killing effect by released payload in target positive tumor cells. *BMC Cancer* **19**:194 10.1186/s12885-019-5336-7.

Cilfone NA, Kirschner DE, and Linderman JJ (2015) Strategies for efficient numerical implementation of hybrid multi-scale agent-based models to describe biological systems. *Cell Mol Bioeng* **8**:119–136 DOI: 10.1007/s12195-014-0363-6.

Cilliers C, Guo H, Liao J, Christodolu N, and Thurber GM (2016) Multiscale modeling of antibody-drug conjugates: connecting tissue and cellular distribution to whole animal pharmacokinetics and potential implications for efficacy. *AAPS J* **18**:1117–1130 DOI: 10.1208/s12248-016-9940-z.

Cilliers C, Menezes B, Nessler I, Linderman J, and Thurber GM (2018) Improved tumor penetration and single-cell targeting of antibody–drug conjugates increases anticancer efficacy and host survival. *Cancer Res* **78**:758–768 DOI: 10.1158/0008-5472.Can-17-1638.

Clardy SM, Yurkovetskiy A, Yin M, Gumerov D, Xu L, Ter-Ovanesyan E, Bu C, Johnson A, Protopopova M, Zhang Q, et al. (2018) Abstract 754: Unique pharmacologic properties of Dolaflexin-based ADCs—a controlled bystander effect. *Cancer Res* **78**(13, Supplement):754 DOI: 10.1158/1538-7445.Am2018-754.

Coats S, Williams M, Kebble B, Dixit R, Tseng L, Yao NS, Tice DA, and Soria JC (2019) Antibody-drug conjugates: future directions in clinical and translational strategies to improve the therapeutic index. *Clin Cancer Res* **25**:5441–5448 DOI: 10.1158/1078-0432.CCR-19-0272.

D'Amico L, Menzel U, Prummer M, Müller P, Buchi M, Kashyap A, Haessler U, Yermanos A, Gébleux R, Briendl M, et al. (2019) A novel anti-HER2 anthracycline-based antibody-drug conjugate induces adaptive anti-tumor immunity and potentiates PD-1 blockade in breast cancer. *J Immunother Cancer* **7**:16 DOI: 10.1186/s40425-018-0464-1.

Eary JF, Schroff RW, Abrams PG, Fritzberg AR, Morgan AC, Kasina S, Reno JM, Srinivasan A, Woodhouse CS, Wilbur DS, et al. (1989) Successful imaging of malignant melanoma with technetium-99m-labeled monoclonal antibodies. *J Nucl Med* **30**:25–32 DOI: http://www.ncbi.nlm.nih.gov/pubmed/2642954.

Erickson HK, Widdison WC, Mayo MF, Whiteman K, Audette C, Wilhelm SD, and Singh R (2010) Tumor delivery and in vivo processing of disulfide-linked and thioether-linked antibody-maytansinoid conjugates. *Bioconjug Chem* **21**:84–92 DOI: 10.1021/bc900315y.

Fujimori K, Covell DG, Fletcher JE, and Weinstein JN (1989) Modeling analysis of the global and microscopic distribution of immunoglobulin G, $F(ab')_2$, and Fab in tumors. *Cancer Res* **49**:5656–5663.

García-Alonso S, Ocaña A, and Pandiella A (2020) Trastuzumab emtansine: mechanisms of action and resistance, clinical progress, and beyond. *Trends Cancer* **6**:130–146 DOI: 10.1016/j.trecan.2019.12.010.

Graff CP and Wittrup KD (2003) Theoretical analysis of antibody targeting of tumor spheroids: importance of dosage for penetration, and affinity for retention. *Cancer Res* **63**:1288–1296 DOI: http://www.ncbi.nlm.nih.gov/entrez/query.fcgi?cmd=Retrieve&db=PubMed&dopt=Citation&list_uids=12649189.

Hamblett KJ, Jacob AP, Gurgel JL, Tometsko ME, Rock BM, Patel SK, Milburn RR, Siu S, Ragan SP, Rock DA, et al. (2015) SLC46A3 is required to transport catabolites of noncleavable antibody maytansine conjugates from the lysosome to the cytoplasm. *Cancer Res* **75**:5329–5340 DOI: 10.1158/0008-5472.CAN-15-1610.

Hilmas DE and Gillette EL (1974) Morphometric analyses of the microvasculature of tumors during growth and after x-irradiation. *Cancer* **33**:103–110.

Hunter FW, Barker HR, Lipert B, Rothé F, Gebhart G, Piccart-Gebhart MJ, Sotiriou C, and Jamieson SMF (2020) Mechanisms of resistance to trastuzumab emtansine (T-DM1) in HER2-positive breast cancer. *Br J Cancer* **122**:603–612 DOI: 10.1038/s41416-019-0635-y.

Ilovich O, Qutaish M, Hesterman JY, Orcutt K, Hoppin J, Polyak I, Seaman M, Abu-Yousif AO, Cvet D, and Bradley DP (2018) Dual-isotope cryoimaging quantitative autoradiography: investigating antibody-drug conjugate distribution and payload delivery through imaging. *J Nucl Med* **59**:1461–1466 DOI: 10.2967/jnumed.118.207753.

Iwata TN, Ishii C, Ishida S, Ogitani Y, Wada T, and Agatsuma T (2018) A HER2-targeting antibody-drug conjugate, trastuzumab deruxtecan (DS-8201a), enhances antitumor immunity in a mouse model. *Mol Cancer Ther* **17**:1494–1503 DOI: 10.1158/1535-7163.MCT-17-0749.

Joslyn LR, Kirschner DE, and Linderman JJ (2020) *CaliPro*: a calibration protocol that utilizes parameter density estimation to explore parameter space and calibrate complex biological models. *Cell Mol Bioeng* **14**:31–47 DOI: 10.1007/s12195-020-00650-z.

Khera E, Cilliers C, Bhatnagar S, and Thurber GM (2018) Computational transport analysis of antibody-drug conjugate bystander effects and payload tumoral distribution: implications for therapy. *Mol Syst Des Eng* **3**:73–88 DOI: 10.1039/c7me00093f.

Khera E, Cilliers C, Smith MD, Ganno ML, Lai KC, Keating TA, Kopp A, Nessler I, Abu-Yousif AO, and Thurber GM (2021) Quantifying ADC bystander payload penetration with cellular resolution using pharmacodynamic mapping. *Neoplasia* **23**:210–221 DOI: 10.1016/j.neo.2020.12.001.

Kovtun YV, Audette CA, Ye Y, Xie H, Ruberti MF, Phinney SJ, Leece BA, Chittenden T, Blättler WA, and Goldmacher VS (2006) Antibody-drug conjugates designed to eradicate tumors with homogeneous and heterogeneous expression of the target antigen. *Cancer Res* **66**:3214–3221 DOI: 10.1158/0008-5472.CAN-05-3973.

Le Joncour V, Martins A, Puhka M, Isola J, Salmikangas M, Laakkonen P, Joensuu H, and Barok M (2019) A novel anti-HER2 antibody-drug conjugate XMT-1522 for HER2-positive breast and gastric cancers resistant to trastuzumab emtansine. *Mol Cancer Ther* **18**:1721–1730 DOI: 10.1158/1535-7163.MCT-19-0207.

Li F, Emmerton KK, Jonas M, Zhang X, Miyamoto JB, Setter JR, Nicholas ND, Okeley NM, Lyon RP, Benjamin DR, et al. (2016) Intracellular released payload influences potency and bystander-killing effects of antibody-drug conjugates in preclinical models. *Cancer Res* **76**:2710–2719 DOI: 10.1158/0008-5472.CAN-15-1795.

Li J, Jiang E, Wang X, Shangguan AJ, Zhang L, and Yu Z (2015) Dormant cells: the original cause of tumor recurrence and metastasis. *Cell Biochem Biophys* **72**:317–320 DOI: 10.1007/s12013-014-0477-4.

Lu G, Fakurnejad S, Martin BA, van den Berg NS, van Keulen S, Nishio N, Zhu AJ, Chirita SU, Zhou Q, Gao RW, et al. (2020a) Predicting therapeutic antibody delivery into human head and neck cancers. *Clin Cancer Res* **26**:2582–2594 DOI: 10.1158/1078-0432.CCR-19-3717.

Lu G, Nishio N, van den Berg NS, Martin BA, Fakurnejad S, van Keulen S, Colevas AD, Thurber GM, and Rosenthal EL (2020b) Co-administered antibody improves penetration of antibody-dye conjugate into human cancers with implications for antibody-drug conjugates. *Nat Commun* **11**:5667 DOI: 10.1038/s41467-020-19498-y.

Maass KF, Kulkarni C, Betts AM, and Wittrup KD (2016) Determination of cellular processing rates for a trastuzumab-maytansinoid antibody-drug conjugate (ADC) highlights key parameters for ADC design. *AAPS J* **18**:635–646 DOI: 10.1208/s12248-016-9892-3.

Manthri S, Singal S, Youssef B, and Chakraborty K (2019) Long-time response with ado-trastuzumab emtansine in a recurrent metastatic breast cancer. *Cureus* **11**:e6036 10.7759/cureus.6036.

Menezes B, Cilliers C, Wessler T, Thurber GM, and Linderman JJ (2020) An agent-based systems pharmacology model of the antibody-drug conjugate kadcyla to predict efficacy of different dosing regimens. *AAPS J* **22**:29 DOI: 10.1208/s12248-019-0391-1.

Nessler I, Khera E, Vance S, Kopp A, Qiu Q, Keating TA, Abu-Yousif AO, Sandal T, Legg J, Thompson L, et al. (2020) Increased tumor penetration of single-domain antibody-drug conjugates improves *in vivo* efficacy in prostate cancer models. *Cancer Res* **80**:1268–1278 DOI: 10.1158/0008-5472.CAN-19-2295.

Ocaña A, Amir E, and Pandiella A (2020) HER2 heterogeneity and resistance to anti-HER2 antibody-drug conjugates. *Breast Cancer Res* **22**:15 DOI: 10.1186/s13058-020-1252-7.

Ogitani Y, Hagihara K, Oitate M, Naito H, and Agatsuma T (2016) Bystander killing effect of DS-8201a, a novel anti-human epidermal growth factor receptor 2 antibody-drug conjugate, in tumors with human epidermal growth factor receptor 2 heterogeneity. *Cancer Sci* **107**:1039–1046 DOI: 10.1111/cas.12966.

Oldham RK, Foon KA, Morgan AC, Woodhouse CS, Schroff RW, Abrams PG, Fer M, Schoenberger CS, Farrell M, Kimball E, et al. (1984) Monoclonal antibody therapy of malignant melanoma: in vivo localization in cutaneous metastasis after intravenous administration. *J Clin Oncol* **2**:1235–1244 DOI: 10.1200/JCO.1984.2.11.1235.

Ponte JF, Lanieri L, Khera E, Laleau R, Ab O, Espelin C, Kohli N, Matin B, Setiady Y, Miller ML, et al. (2021) Antibody co-administration can improve systemic and local distribution of antibody drug conjugates to increase in vivo efficacy. *Mol Cancer Ther* **20**:203–212. DOI: 10.1158/1535-7163.MCT-20-0451.

Rhoden JJ and Wittrup KD (2012) Dose dependence of intratumoral perivascular distribution of monoclonal antibodies. *J Pharm Sci* **101**:860–867 DOI: 10.1002/jps.22801.

Rios-Doria J, Harper J, Rothstein R, Wetzel L, Chesebrough J, Marrero A, Chen C, Strout P, Mulgrew K, McGlinchey K, et al. (2017) Antibody-drug conjugates bearing pyrrolobenzodiazepine or tubulysin payloads are immunomodulatory and synergize with multiple immunotherapies. *Cancer Res* **77**:2686–2698 DOI: 10.1158/0008-5472.CAN-16-2854.

Ríos-Luci C, García-Alonso S, Díaz-Rodríguez E, Nadal-Serrano M, Arribas J, Ocaña A, and Pandiella A (2017) Resistance to the antibody-drug conjugate T-DM1 is based in a reduction in lysosomal proteolytic activity. *Cancer Res* **77**:4639–4651 DOI: 10.1158/0008-5472.CAN-16-3127.

Rye IH, Trinh A, Saetersdal AB, Nebdal D, Lingjaerde OC, Almendro V, Polyak K, Børresen-Dale AL, Helland Å, Markowetz F, et al. (2018) Intratumor heterogeneity defines treatment-resistant HER2+ breast tumors. *Mol Oncol* **12**:1838–1855 DOI: 10.1002/1878-0261.12375.

Scott AM, Lee FT, Jones R, Hopkins W, MacGregor D, Cebon JS, Hannah A, Chong G, U P, Papenfuss A, et al. (2005) A phase I trial of humanized monoclonal antibody A33 in patients with colorectal carcinoma: biodistribution, pharmacokinetics, and quantitative tumor uptake. *Clin Cancer Res* **11**:4810–4817 DOI: 10.1158/1078-0432.CCR-04-2329.

Seol H, Lee HJ, Choi Y, Lee HE, Kim YJ, Kim JH, Kang E, Kim SW, and Park SY (2012) Intratumoral heterogeneity of HER2 gene amplification in breast cancer: its clinicopathological significance. *Mod Pathol* **25**:938–948 DOI: 10.1038/modpathol.2012.36.

Shah DK, Haddish-Berhane N, and Betts A (2012) Bench to bedside translation of antibody drug conjugates using a multiscale mechanistic PK/PD model: a case study with brentuximab-vedotin. *J Pharmacokinet Pharmacodyn* **39**:643–659 DOI: 10.1007/s10928-012-9276-y.

Singh AP, Guo L, Verma A, Wong GG, Thurber GM, and Shah DK (2020a) Antibody coadministration as a strategy to overcome binding-site barrier for ADCs: a quantitative investigation. *AAPS J* **22**:28 DOI: 10.1208/s12248-019-0387-x.

Singh AP, Maass KF, Betts AM, Wittrup KD, Kulkarni C, King LE, Khot A, and Shah DK (2016) Evolution of antibody-drug conjugate tumor disposition model to predict preclinical tumor pharmacokinetics of trastuzumab-emtansine (T-DM1). *AAPS J* **18**:861–875 DOI: 10.1208/s12248-016-9904-3.

Singh AP, Seigel GM, Guo L, Verma A, Wong GG, Cheng HP, and Shah DK (2020b) Evolution of the systems pharmacokinetics-pharmacodynamics model for antibody-drug conjugates to characterize tumor heterogeneity and *in vivo* bystander effect. *J Pharmacol Exp Ther* **374**:184–199 DOI: 10.1124/jpet.119.262287.

Singh AP and Shah DK (2017) Application of a PK-PD modeling and simulation-based strategy for clinical translation of antibody-drug conjugates: a case study with trastuzumab emtansine (T-DM1). *AAPS J* **19**:1054–1070 DOI: 10.1208/s12248-017-0071-y.

Staudacher AH and Brown MP (2017) Antibody drug conjugates and bystander killing: is antigen-dependent internalisation required? *Br J Cancer* **117**:1736–1742 DOI: 10.1038/bjc.2017.367.

Thuss-Patience PC, Shah MA, Ohtsu A, Van Cutsem E, Ajani JA, Castro H, Mansoor W, Chung HC, Bodoky G, Shitara K, et al. (2017) Trastuzumab emtansine versus taxane use for previously treated HER2-positive locally advanced or metastatic gastric or gastro-oesophageal junction adenocarcinoma (GATSBY): an international randomised, open-label, adaptive, phase 2/3 study. *Lancet Oncol* **18**:640–653 DOI: 10.1016/S1470-2045(17)30111-0.

van Geel R, Wijdeven MA, Heesbeen R, Verkade JM, Wasiel AA, van Berkel SS, and van Delft FL (2015) Chemoenzymatic conjugation of toxic payloads to the globally conserved N-glycan of native mAbs provides homogeneous and highly efficacious antibody-drug conjugates. *Bioconjug Chem* **26**:2233–2242 DOI: 10.1021/acs.bioconjchem.5b00224.

Vasalou C, Helmlinger G, and Gomes B (2015) A mechanistic tumor penetration model to guide antibody drug conjugate design. *PLoS One* **10**:e0118977 DOI: 10.1371/journal.pone.0118977.

Williams LE, Duda RB, Proffitt RT, Beatty BG, Beatty JD, Wong JYC, Paxton RJ (1988) Tumor uptake as a function of tumor mass - a mathematical model. *J Nucl Med* **29**:103–109.

Yardley DA, Kaufman PA, Huang W, Krekow L, Savin M, Lawler WE, Zrada S, Starr A, Einhorn H, Schwartzberg LS, et al. (2015) Quantitative measurement of HER2 expression in breast cancers: comparison with 'real-world' routine HER2 testing in a multicenter Collaborative Biomarker Study and correlation with overall survival. *Breast Cancer Res* **17**:41 DOI: 10.1186/s13058-015-0543-x.

Address correspondence to: Jennifer J. Linderman, University of Michigan, 2800 Plymouth Rd., Ann Arbor, MI 48109. E-mail: linderma@umich.edu; or Greg M. Thurber, University of Michigan, 2800 Plymouth Rd., Ann Arbor, MI 48109. E-mail: gthurber@umich.edu